Mixing Estimates for Estuaries

HANS BURCHARD, XAVER LANGE, AND KNUT KLINGBEIL

Leibniz Institute for Baltic Sea Research Warnemünde, Rostock, Germany

PARKER MACCREADY

University of Washington, Seattle, Washington

(Manuscript received 19 July 2018, in final form 13 October 2018)

ABSTRACT

The well-known Knudsen relations and the total exchange flow (TEF) analysis framework provide quantifications of exchange flow across an open boundary to the adjacent ocean in terms of bulk values (Knudsen theory: inflow and outflow volume or salinity) or with resolution in salinity space (TEF: profiles of volume and salt flux in salinity coordinates). In the present study, these theories are extended toward mixing of salinity, defined as the decay of salinity variance due to turbulent mixing. In addition to the advective fluxes, diffusive fluxes across the boundary are also considered now. These new Knudsen and TEF relations for mixing are derived by applying Gauss's theorem to the salinity square and salinity variance equations. As a result of the analysis, four different Knudsen relations for the mixing in estuaries are derived. The first one is exact and considers nonperiodicity as well as nonconstancy of the inflow and outflow salinities. The other three formulations are approximate only, in the sense that either nonperiodicity or nonconstancy or both are relaxed. The simplest of those formulations has recently been derived by MacCready et al. and estimates the estuarine mixing as the product of inflow salinity, outflow salinity, and time-averaged river runoff. These four mixing estimates are systematically assessed by means of a number of idealized estuarine test cases. For periodic tidal flow, the simplest estimate still predicts the effective (physical plus numerical) mixing within an error of about 10%.

1. Introduction

Estuaries can be regarded as mixing zones which dilute saltwater inflowing from the ocean with freshwater from river runoff to produce brackish water flowing back into the ocean (Fischer 1976). To underline this key estuarine function, Wang et al. (2017) used the name *mixing machine* to characterize estuarine dynamics. Since mixing is such a fundamental property in estuaries, several authors have proposed quantitative measures for it. In an early estuarine model, Hansen and Rattray (1965) quantified mixing in terms of a constant eddy diffusivity to parameterize tidal mixing. This was also used by Hetland and Geyer (2004) to show how increased eddy diffusivity results in a decreased length of the estuarine brackish water zone. One limitation of eddy diffusivity as a measure of estuarine mixing is that it represents for a tracer the ratio of the turbulent flux and the vertical gradient, the estuarine-wide average of which has no physical significance. Second, eddy diffusivity may be specifically high at unstratified locations where no mixing is taking place since the waters are already mixed, as, for example, in the freshwater region or the bottom boundary layer. For the same reason, the turbulent dissipation rate which can directly be measured and often is used to indicate mixing (Peters and Bokhorst 2000) is not suitable to quantify estuarine mixing. Another candidate for quantifying estuarine mixing could be the turbulent buoyancy flux (Peters and Bokhorst 2001), which, however, is a vectorial quantity where opposing contributions might partially compensate each other. This occurs, for example, in tidal flow with downward buoyancy flux during ebb and upward buoyancy flux during flood, although mixing of salt occurs in both situations. An interesting alternative might be to use

Denotes content that is immediately available upon publication as open access.

Corresponding author: Hans Burchard, hans.burchard@io-warnemuende.de

DOI: 10.1175/JPO-D-18-0147.1

diahaline salt fluxes as measure for mixing, as proposed by Walin (1977).

Physically, mixing occurs on the microscale, when small-scale tracer gradients caused by turbulent stirring are smoothed by the divergence of molecular tracer fluxes. This molecular mixing is quantified as the scalar dissipation rate of tracer variance per unit volume, $\chi^c = 2\nu^c(\overline{\nabla c'})^2$ (Umlauf and Burchard 2005), where ν^c is the molecular tracer diffusivity, $\nabla c'$ is the gradient of the turbulent tracer fluctuation, and the overbar denotes an ensemble average (Lesieur 1997). Therefore, Burchard and Rennau (2008) proposed to use the volume integral of χ^c as a measure for basin-wide mixing, a quantity which can easily be calculated from numerical model results. This method was first applied by Burchard et al. (2009) to quantify salt mixing in a coastal ocean simulation of the western Baltic Sea. A first application of the salinity variance dissipation to estuarine mixing has recently been demonstrated by Wang et al. (2017) using the total exchange flow (TEF) analysis framework of MacCready (2011). Burchard and Rennau (2008) also showed how the effective (physical plus numerical) mixing can be consistently quantified locally for numerical simulations, such that the integral of the sum of both gives the effective total mixing. This model analysis method has later been refined by Klingbeil et al. (2014), including a numerical analysis for a model simulation of the western Baltic Sea. A first numerical mixing analysis for estuaries using these methods has recently been carried out by Ralston et al. (2017), who proposed to reduce physical mixing such that the effective mixing remains at realistic levels.

Knudsen (1900) formulated volume flux and salt flux relations for freshwater, saltwater, and brackish water in estuaries to quantify this water mass transformation. He also mentioned that mixing is responsible for the transformation, but neither defined nor quantified the mixing itself. While Knudsen (1900) limited his early theory to bulk values of inflowing and outflowing salinities and transports of volume and salt, Walin (1977) much later introduced an isohaline framework to describe volume, salt, and tracer transports with resolution in salinity space. Following a similar concept, MacCready (2011) introduced the TEF analysis framework providing volume and salt transport as functions of salinity classes. Moreover, he connected the TEF concept to the Knudsen quantities of inflow and outflow salinities and net transports per salinity class in a consistent way. Wang et al. (2017) showed for a numerical model study of the Hudson River estuary how the effective mixing integrated over an estuarine control volume can be quantified by means of the TEF concept.

In their recent review, Burchard et al. (2018) applied the Knudsen relations and the TEF analysis framework to the multidecadal inflow dynamics of the Baltic Sea, refining earlier short-term studies by Walin (1981). The review by Burchard et al. (2018) additionally provides a translation of the Knudsen (1900) paper into English. The TEF framework is also used to track reactive biogeochemical tracers such as nutrients and dissolved oxygen in large estuarine systems.

Based on the Knudsen relations and the TEF analysis framework, MacCready et al. (2018) derived a quantification for time-averaged and volume-integrated estuarine mixing as the product of the inflow salinity, the outflow salinity, and the time-averaged river runoff.

The present manuscript adds the following aspects to the new theory of MacCready et al. (2018):

1) An exact Knudsen mixing relation is formulated from which the Knudsen mixing relation by MacCready et al. (2018) and other approximate relations are derived by assuming periodic estuarine volume, salt content, and salt variance (or salt square) and/or constancy of the inflow and outflow salinities.
2) The TEF analysis framework developed by MacCready (2011) is used to consistently derive these relations. This particularly leads to the distinction between the square of the characteristic outflow or inflow salinity and the characteristic outflow or inflow salinity squares.
3) In addition to advective fluxes, diffusive fluxes of salt, salt square, and salt variance are included into the TEF concept.
4) The TEF relations are discretized in such a way that they are fully consistent with the effective (physical plus numerical) mixing in the model.

To set the scene, section 2 uses a stationary box estuary to link the Knudsen relations to estuarine mixing and to derive in a simple way the mixing relation introduced by MacCready et al. (2018). A detailed derivation of mixing estimates for general time-dependent estuaries based on mass and salt conservation is then given in section 3. The performance of the derived mixing estimates is investigated in section 4, with two analytical scenarios directly prescribing the exchange flow at an estuarine transect without considering the estuary itself. Scenarios explicitly including estuarine mixing are assessed, using a one-dimensional longitudinal estuary model as well as a two-dimensional model (including vertical resolution). The results and their implications are discussed in section 5 and some conclusions are drawn in section 6.

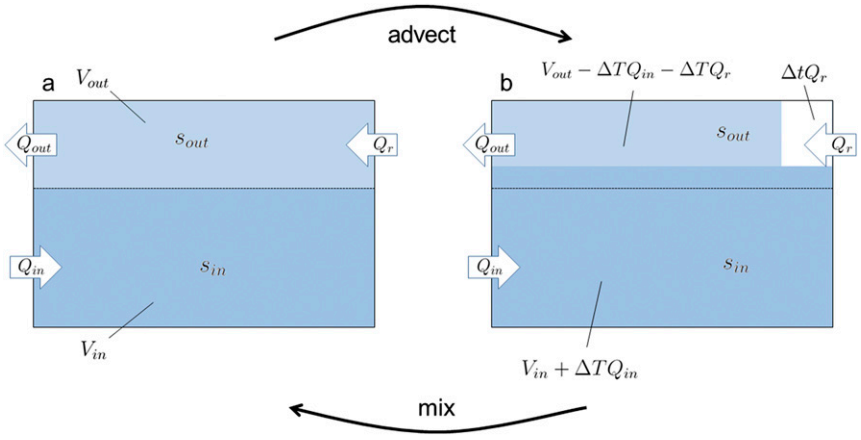

FIG. 1. Schematic box estuary to demonstrate the Knudsen relation for estuarine mixing. (a) Box estuary in basic state when salinities in inflow and outflow boxes are mixed. (b) Box estuary after adiabatic volume and salt fluxes have been applied for a period ΔT, indicating how salinity would be distributed without mixing. In both cases, blue colors qualitatively indicate salinity (white is for zero salinity). Volume fractions before and after adiabatic inflows are indicated as well.

2. A mechanistic model of estuarine mixing

We use here a simple box-type estuary model as prototype of an estuarine mixing machine to motivate the estuarine mixing relation which has recently been introduced by MacCready et al. (2018). This box model is similar to the estuary box model introduced as river boundary condition in climate models (Sun et al. 2017). The model has a lower layer of volume V_{in} with salinity s_{in} and an upper layer of volume V_{out} with salinity s_{out}, with the constant total volume $V = V_{\text{in}} + V_{\text{out}}$ (see Fig. 1a). The lower box has a saline inflow of Q_{in} with salinity s_{in} and the upper layer has a freshwater inflow Q_r and a saline outflow of Q_{out} with salinity s_{out}. In this simple box model with only two water masses, the lower salinity equals the inflow salinity s_{in} and the upper salinity equals the outflow salinity s_{out}. Inflows (generally Q_r and Q_{in}) have a positive sign and outflows (generally Q_{out}) have a negative sign. Under these circumstances, assuming a steady state or periodic variability in time, the transports fulfill the following balances of volume,

$$Q_{\text{in}} + Q_{\text{out}} + Q_r = 0, \tag{1}$$

and salt,

$$Q_{\text{in}} s_{\text{in}} + Q_{\text{out}} s_{\text{out}} = 0. \tag{2}$$

Combining (1) and (2), the well-known Knudsen (1900) relations can be derived:

$$Q_{\text{in}} = \frac{s_{\text{out}}}{s_{\text{in}} - s_{\text{out}}} Q_r, \quad Q_{\text{out}} = -\frac{s_{\text{in}}}{s_{\text{in}} - s_{\text{out}}} Q_r, \tag{3}$$

which means that by only knowing the freshwater runoff and representative inflow and outflow salinities, inflow and outflow volumes can be estimated. In the same way, stationary budgets of salinity square,

$$Q_{\text{in}} (s_{\text{in}})^2 + Q_{\text{out}} (s_{\text{out}})^2 = s_{\text{in}} s_{\text{out}} Q_r, \tag{4}$$

and salinity variance per unit volume,

$$Q_{\text{in}} (s_{\text{in}} - \bar{s})^2 + Q_{\text{out}} (s_{\text{out}} - \bar{s})^2 + Q_r \bar{s}^2 = s_{\text{in}} s_{\text{out}} Q_r, \tag{5}$$

can be derived from (1) and (2), where $\bar{s} = (s_{\text{in}} V_{\text{in}} + s_{\text{out}} V_{\text{out}})/V$ is the mean salinity in the box estuary. Both the balances of the squared salinity and the salinity variance per unit volume are not closed, since they include a source of $s_{\text{in}} s_{\text{out}} Q_r$ on the right-hand side. To guarantee stationary conditions also for these balances, an internal sink term $M = s_{\text{in}} s_{\text{out}} Q_r$ needs to be assumed. Since (5) suggests that this term is an internal sink to salinity variance, M can be interpreted as volume-integrated salinity mixing (Burchard et al. 2009). This is exactly the key result by MacCready et al. (2018): estuarine mixing can be estimated as the product of inflow and outflow salinities with the freshwater runoff.

Using the box-type estuary, we demonstrate this mixing relation geometrically, allowing time dependence. For simplicity, we restrict ourselves to the budget of the squared salinity shown in (4). Application of the salinity-square fluxes from (4) for the short time ΔT without internal mixing (advection step, see Fig. 1) would increase volume-integrated salinity square from

$$Vs_a^2 = (s_{\text{in}})^2 V_{\text{in}} + (s_{\text{out}})^2 V_{\text{out}} \tag{6}$$

to

$$Vs_b^2 = (s_{\text{in}})^2 (V_{\text{in}} + \Delta T Q_{\text{in}}) + (s_{\text{out}})^2 (V_{\text{out}} - \Delta T Q_{\text{in}} - \Delta T Q_r), \tag{7}$$

such that the mixing M required to mix this back to the initial state (mixing step, see Fig. 1) would be

$$M = V \frac{s_b^2 - s_a^2}{\Delta T} = [(s_{\text{in}})^2 - (s_{\text{out}})^2] Q_{\text{in}} - (s_{\text{out}})^2 Q_r = s_{\text{in}} s_{\text{out}} Q_r, \tag{8}$$

where we used the first relation of (3) for the last step. Since the result for M is independent of ΔT, it is also valid for $\Delta T \to 0$. Thus, in this stationary case without temporal and spatial salinity variation within inflowing and outflowing waters, the simple mixing relation of MacCready et al. (2018),

$$M = s_{\text{in}} s_{\text{out}} Q_r, \tag{9}$$

holds exactly.

With s_{in} being the salinity input to the system, which does not depend on the dynamics inside the estuary itself, s_{out} can be calculated as function of mixing, runoff and input salinity:

$$s_{\text{out}} = \frac{M}{s_{\text{in}} Q_r}, \tag{10}$$

such that the ratio of outflowing and inflowing salinity,

$$\text{Mc} = \frac{s_{\text{out}}}{s_{\text{in}}} = \frac{M}{(s_{\text{in}})^2 Q_r} = -\frac{Q_{\text{in}}}{Q_{\text{out}}}, \tag{11}$$

can be regarded as a measure of the estuarine bulk mixing completeness, where $(s_{\text{in}})^2 Q_r$ is the maximum possible mixing (MacCready et al. 2018). It should be noted that the relation $s_{\text{out}}/s_{\text{in}} = -Q_{\text{in}}/Q_{\text{out}}$ had already been formulated by Knudsen (1900).

The usefulness of this simple estimate for the mixing M can be readily shown for real estuaries, if some estimates for inflow and outflow salinity and runoff are available. Since Knudsen (1900) developed his theory for the Baltic Sea, first Baltic Sea mixing estimates are made here. Knudsen (1900) gave the following inflow and outflow salinities obtained from single observations: $s_{\text{in}} = 17.4\,\text{g kg}^{-1}$ and $s_{\text{out}} = 8.7\,\text{g kg}^{-1}$ (giving a mixing completeness of Mc = 50%). Together with the long-term runoff of the Baltic Sea of $Q_r = 15\,252\,\text{m}^3\,\text{s}^{-1}$ (Matthäus and Schinke 1999), this would result in an integrated mixing of $M = s_{\text{in}} s_{\text{out}} Q_r = 2.31 \times 10^6\,\text{m}^3\,\text{s}^{-1}\,(\text{g kg}^{-1})^2$. A more representative estimate may be given based on the model results by Burchard et al. (2018). Over an averaging period of 66 years (1948–2013), the following values were calculated for the straits connecting the Baltic Sea to the rest of the ocean, the Darss Sill (denoted by A here, their Fig. 5) and the Drogden Sill (denoted by B here, their Fig. 6):

A: $Q_{\text{in}}^{\text{A}} = 8022\,\text{m}^3\,\text{s}^{-1}$, $Q_{\text{out}}^{\text{A}} = -17\,774\,\text{m}^3\,\text{s}^{-1}$, $s_{\text{in}}^{\text{A}} = 14.60\,\text{g kg}^{-1}$, $s_{\text{out}}^{\text{A}} = 8.81\,\text{g kg}^{-1}$;
B: $Q_{\text{in}}^{\text{B}} = 8164\,\text{m}^3\,\text{s}^{-1}$, $Q_{\text{out}}^{\text{B}} = -14\,510\,\text{m}^3\,\text{s}^{-1}$, $s_{\text{in}}^{\text{B}} = 18.54\,\text{g kg}^{-1}$, $s_{\text{out}}^{\text{B}} = 8.49\,\text{g kg}^{-1}$.

Due to the long term integration, storage terms can be neglected. With this,

$$s_{\text{in}} = \frac{Q_{\text{in}}^{\text{A}} s_{\text{in}}^{\text{A}} + Q_{\text{in}}^{\text{B}} s_{\text{in}}^{\text{B}}}{Q_{\text{in}}^{\text{A}} + Q_{\text{in}}^{\text{B}}}, \qquad s_{\text{out}} = \frac{Q_{\text{out}}^{\text{A}} s_{\text{out}}^{\text{A}} + Q_{\text{out}}^{\text{B}} s_{\text{out}}^{\text{B}}}{Q_{\text{out}}^{\text{A}} + Q_{\text{out}}^{\text{B}}}, \tag{12}$$

such that $s_{\text{in}} = 16.59\,\text{g kg}^{-1}$ and $s_{\text{out}} = 8.67\,\text{g kg}^{-1}$ (resulting in a mixing completeness of Mc = 54%), and with $Q_r = -(Q_{\text{in}}^{\text{A}} + Q_{\text{in}}^{\text{B}} + Q_{\text{out}}^{\text{A}} + Q_{\text{out}}^{\text{B}}) = 16\,098\,\text{m}^3\,\text{s}^{-1}$, an estimated mixing rate of $M = 2.32 \times 10^6\,\text{m}^3\,\text{s}^{-1}\,(\text{g kg}^{-1})^2$ results. It certainly is coincidence that both estimates are so close to each other, but quite likely the real long-term mixing of the Baltic Sea is on the order of $M \approx 2 \times 10^6\,\text{m}^3\,\text{s}^{-1}\,(\text{g kg}^{-1})^2$. Future research will challenge these mixing estimates.

3. Derivation of an exact mixing relation using TEF

Here, the TEF analysis framework first described by MacCready (2011) for volume and salinity is extended to squared salinity and salinity variance. The framework is derived from the Reynolds-averaged continuity equation,

$$\partial_x u + \partial_y v + \partial_z w = 0, \tag{13}$$

and the Reynolds-averaged salinity equation using the eddy diffusivity assumption for turbulent salinity fluxes,

$$\partial_t s + \partial_x (us) + \partial_y (vs) + \partial_z (ws) - \partial_x (K_h \partial_x s) - \partial_y (K_h \partial_y s) - \partial_z (K_v \partial_z s) = 0. \tag{14}$$

Cartesian coordinates are used, with time t, the space vector (x, y, z), and the velocity vector (u, v, w). Horizontal and vertical eddy diffusivities are denoted by K_h and K_v, respectively, and s is salinity. Kinematic boundary conditions are applied, that is, there is no

volume flux through the surface at $z = \eta$ and the bottom at $z = -H$. This implies that precipitation and evaporation are neglected (Klingbeil et al. 2018). Consequently, surface and bottom salinity fluxes are set to zero.

Carrying out a volume integration of (13), the volume budget of an estuary can be expressed as

$$\partial_t V = -\int_{A(0)} u_n \, dA - \int_{A_r} u_n \, dA, \tag{15}$$

where $A(0)$ is the open-boundary transect area (which may be composed of several separate subareas) for salinities larger than zero typically located at the open boundary, and A_r is the area through which freshwater of zero salinity is discharged into the control volume. More generally, we define $A(S)$ as the part of the open-boundary transect with salinities s larger than a specific salinity S, $s > S$. Furthermore, u_n is the normal velocity component (positive outwards). Similarly, volume integration of the salinity equation in (14) results in

$$\partial_t \int_V s \, dV = -\int_{A(0)} (u_n s - K_h \partial_n s) \, dA, \tag{16}$$

where $\partial_n s$ denotes the salinity gradient normal to the transect $A(0)$ (pointing outward).

For any tracer c, the total (advective plus diffusive) outward tracer flux F^c can be defined at the open boundary to allow for the inclusion of diffusive cross-boundary tracer fluxes into the Knudsen (1900) and MacCready (2011) theorems:

$$F^c = u_n c - K_h \partial_n c, \tag{17}$$

with $F^1 = u_n$ being the volume flux. Using (17), the volume-integrated salinity budget in (16) can be rewritten as

$$\partial_t \int_V s \, dV = -\int_{A(0)} F^s \, dA. \tag{18}$$

If we now multiply (14) by $2s$, we obtain a salinity-squared equation:

$$\begin{aligned} &\partial_t s^2 + \partial_x(us^2) + \partial_y(vs^2) + \partial_z(ws^2) - \partial_x(K_h \partial_x s^2) \\ &\quad - \partial_y(K_h \partial_y s^2) - \partial_z(K_v \partial_z s^2) = -\chi^s \end{aligned} \tag{19}$$

with the local salt mixing

$$\chi^s = 2[K_h(\partial_x s)^2 + K_h(\partial_y s)^2 + K_v(\partial_z s)^2]; \tag{20}$$

see Burchard and Rennau (2008). Integrating the s^2 equation [(19)] over the total volume V results in

$$\partial_t \int_V s^2 \, dV = -\int_{A(0)} F^{s^2} \, dA - M, \tag{21}$$

with the volume-integrated mixing

$$M = \int_V \chi^s \, dV, \tag{22}$$

and the effective flux of squared salinity at the open boundary F^{s^2}. Combining (14) and (19), a budget equation for the salinity variance is derived:

$$\partial_t \int_V s'^2 \, dV = -\int_{A(0)} F^{s'^2} \, dA - \overline{s}^2 \int_{A_r} u_n \, dA - M, \tag{23}$$

with the salinity deviation $s' = s - \overline{s}$, where $\overline{s} = (1/V)\int_V s \, dV$ is the volume-averaged salinity and $F^{s'^2}$ is the effective flux of salinity variance at the open boundary. To derive (23), budget equations for the mean salinity $\overline{s}$ and its square $\overline{s}^2$ are derived by using (15) and (18). Based on this, a budget equation for the variance per unit volume, s'^2 is derived, which is then volume integrated [see (2) and (3) of MacCready et al. (2018)]. The boundary flux of s'^2 is finally split between open boundaries with $s > 0$ and river boundaries with $s = 0$. Compared to the volume-integrated budget of the squared salinity from (21), the variance budget in (23) is additionally increased by freshwater input (second term on right-hand side). The salinity variance budget is more clearly related to the concept of molecular mixing, and it highlights the importance of the river flow as a source of unmixed, high-variance water. On the other hand, the salinity-squared budget arrives at the same net mixing M, and in a steady state it relies only on information at the ocean boundary section, not the whole estuarine volume. This makes the salinity-squared formalism potentially easier to apply to analysis of observations.

For any tracer c, its time-averaged boundary flux can be expressed in salinity coordinates:

$$-\left\langle \int_{A(0)} F^c \, dA \right\rangle = Q^c(0) = \int_0^{s_{\max}} q^c(s) \, ds \tag{24}$$

with

$$q^c(S) = -\frac{\partial Q^c(S)}{\partial S} \quad \text{and} \quad Q^c(S) = -\left\langle \int_{A(S)} F^c \, dA \right\rangle, \tag{25}$$

where angle brackets denote temporal averaging. In (25), $Q^c(S)$ is the incoming transport of c through the cross-sectional area $A(S)$ with salinities s higher than S, and $q^c(S)$ is the incoming boundary flux of c per salinity class.

Bulk values for inflow and outflow of any tracer c can be defined:

$$Q^c_{\text{in}} = \int_0^{S_{\max}} (q^c)^+ \, dS \geq 0;$$
$$Q^c_{\text{out}} = \int_0^{S_{\max}} (q^c)^- \, dS \leq 0, \tag{26}$$

where for any function a, the positive part is calculated as $(a)^+ = \max(a, 0)$ and the negative part is calculated as $a^- = \min(a, 0)$, resulting in positive inflow transports and negative outflow transports. For the volume fluxes with $c = 1$, we write for simplicity $q = q^1$ and $Q = Q^1$. The tracer c could be any tracer, including reactive tracers such as biogeochemical constituents or radioactively decaying tracers (Walin 1977). In the following, we will use $c = s$ for salinity transports, $c = s^2$ for salinity-square transports, and $c = s'^2$ for transport of salinity variance per unit volume.

When numerically calculating the inflow and outflow transports in well-mixed conditions, the algorithm in (26) has been found to be numerically noisy, giving inconsistent results for different numbers of salinity bins. Therefore, MacCready et al. (2018) propose for the basic situation of inflow at high salinities and outflow at low salinities to determine the dividing salinity S_{div} at which $Q^c(S)$ has its maximum. Parameter Q^c_{in} is then calculated as $Q^c(S_{\text{div}})$.

Based on the definitions in (26), the tracer concentrations representative for inflow and outflow are calculated as

$$c_{\text{in}} = \frac{Q^c_{\text{in}}}{Q_{\text{in}}}; \quad c_{\text{out}} = \frac{Q^c_{\text{out}}}{Q_{\text{out}}}. \tag{27}$$

Equations (24)–(27) are a generalization of the TEF concept of MacCready (2011). For salinity s, the identity of Q^s_{in} and Q^s_{out} from (26) and the inflow and outflow salinities F_{in} and F_{out} as defined by MacCready (2011) have already been shown by Burchard et al. (2018, see their appendix C). Similarly, this identity could also be shown for any tracer c.

In the following, a key issue will be the general inequality of $(s^2)_{\text{in}}$ and $(s_{\text{in}})^2$ as well as of $(s^2)_{\text{out}}$ and $(s_{\text{out}})^2$. To derive a condition for their equality, we calculate

$$\begin{aligned}
(s^2)_{\text{in}} = (s_{\text{in}})^2 \;&\Rightarrow \int_0^{S_{\max}} q^+ \, dS \int_0^{S_{\max}} q^+ S^2 \, dS = \left(\int_0^{S_{\max}} q^+ S \, dS \right)^2, \\
(s^2)_{\text{out}} = (s_{\text{out}})^2 \;&\Rightarrow \int_0^{S_{\max}} q^- \, dS \int_0^{S_{\max}} q^- S^2 \, dS = \left(\int_0^{S_{\max}} q^- S \, dS \right)^2,
\end{aligned} \tag{28}$$

where the latter equalities are only given if s is constant over the positive and constant over the negative ranges of q. Therefore, we call this condition the constancy condition. This is true in the box estuary case (section 2), but is generally not valid.

The temporally averaged freshwater runoff is defined as

$$Q_r = -\left\langle \int_{A_r} u_n \, dA \right\rangle. \tag{29}$$

With (24) and after temporal averaging, the volume-integrated budgets in (15), (16), and (21) can be rewritten as

$$\begin{aligned}
V_{\text{stor}} = \langle \partial_t V \rangle &= \int_0^{S_{\max}} q(S) \, dS + Q_r \\
&= Q_{\text{in}} + Q_{\text{out}} + Q_r,
\end{aligned} \tag{30}$$

$$\begin{aligned}
S_{\text{stor}} = \langle \partial_t (\overline{s} V) \rangle &= \left\langle \partial_t \int_V s \, dV \right\rangle = \int_0^{S_{\max}} q^s(S) \, dS \\
&= Q_{\text{in}} s_{\text{in}} + Q_{\text{out}} s_{\text{out}},
\end{aligned} \tag{31}$$

$$\begin{aligned}
(S^2)_{\text{stor}} = \left\langle \partial_t (\overline{s^2} V) \right\rangle &= \left\langle \partial_t \int_V s^2 \, dV \right\rangle = \int_0^{S_{\max}} q^{s^2}(S) \, dS - \langle M \rangle \\
&= Q_{\text{in}} (s^2)_{\text{in}} + Q_{\text{out}} (s^2)_{\text{out}} - \langle M \rangle,
\end{aligned} \tag{32}$$

and

$$\begin{aligned}
(S'^2)_{\text{stor}} = \left\langle \partial_t (\overline{s'^2} V) \right\rangle &= \left\langle \partial_t \int_V s'^2 \, dV \right\rangle \\
&= \int_0^{S_{\max}} q^{s'^2}(s) \, ds - \left\langle \overline{s}^2 \int_{A_r} u_n \, dA \right\rangle - \langle M \rangle \\
&= Q_{\text{in}} (s'^2)_{\text{in}} + Q_{\text{out}} (s'^2)_{\text{out}} - \left\langle \overline{s}^2 \int_{A_r} u_n \, dA \right\rangle - \langle M \rangle,
\end{aligned} \tag{33}$$

where $\overline{s^2}$ is the volume-averaged salinity square and $\overline{s'^2}$ is the volume-averaged salinity variance, and V_{stor}, S_{stor}, $(S^2)_{\text{stor}}$ and $(S'^2)_{\text{stor}}$ are the storage terms for volume, salinity, salinity-squared, and salinity variance. These vanish in case of periodicity. The variance budget in (33) includes the temporal covariance between the square of

the mean salinity and the freshwater runoff, as seen in the second-to-last term. A stationary version of (33) has already been derived for the box estuary in (5). Combining (30) and (31), we obtain the time-dependent versions of the Knudsen relations [see (3)]:

$$Q_{\text{out}} = -\frac{s_{\text{in}}}{s_{\text{in}} - s_{\text{out}}} Q_R + \frac{s_{\text{in}}}{s_{\text{in}} - s_{\text{out}}} V_{\text{stor}} - \frac{1}{s_{\text{in}} - s_{\text{out}}} S_{\text{stor}}, \tag{34}$$

$$Q_{\text{in}} = \frac{s_{\text{out}}}{s_{\text{in}} - s_{\text{out}}} Q_R - \frac{s_{\text{out}}}{s_{\text{in}} - s_{\text{out}}} V_{\text{stor}} + \frac{1}{s_{\text{in}} - s_{\text{out}}} S_{\text{stor}}. \tag{35}$$

Assuming periodicity of the volume and salt budgets, (30) and (31), the Knudsen (1900) relations (1)–(3) are readily obtained. Under these conditions, the total volume transport equals the (negative) runoff, $Q(0) = -Q_r$, and the total salt transport vanishes, $Q^s(0) = 0$.

From (34) and (35) in combination with (32), a hierarchy of four different Knudsen relations for mixing can be derived, depending on the assumption of periodicity and constancy.

1) We obtain an exact Knudsen relation for mixing by allowing nonconstancy [$(s^2)_{\text{in}} \neq (s_{\text{in}})^2$ and $(s^2)_{\text{out}} \neq (s_{\text{out}})^2$] and nonperiodicity:

$$\langle M \rangle = M_e = \frac{s_{\text{out}}(s^2)_{\text{in}} - s_{\text{in}}(s^2)_{\text{out}}}{s_{\text{in}} - s_{\text{out}}} (Q_r - V_{\text{stor}}) + \frac{(s^2)_{\text{in}} - (s^2)_{\text{out}}}{s_{\text{in}} - s_{\text{out}}} S_{\text{stor}} - (S^2)_{\text{stor}}. \tag{36}$$

2) For the case of constancy [$(s^2)_{\text{in}} = (s_{\text{in}})^2$ and $(s^2)_{\text{out}} = (s_{\text{out}})^2$] as in the box estuary case of section 2, (36) may be simplified to the approximate, constant, and nonperiodic Knudsen relation

$$\langle M \rangle \approx M_c = s_{\text{in}} s_{\text{out}} (Q_r - V_{\text{stor}}) + (s_{\text{in}} + s_{\text{out}}) S_{\text{stor}} - (S^2)_{\text{stor}}. \tag{37}$$

3) Assuming periodicity, but allowing nonconstancy, an approximate, nonconstant, and periodic Knudsen relation for the mixing is obtained from (36):

$$\langle M \rangle \approx M_p = \frac{s_{\text{out}}(s^2)_{\text{in}} - s_{\text{in}}(s^2)_{\text{out}}}{s_{\text{in}} - s_{\text{out}}} Q_r. \tag{38}$$

4) Assuming again constancy, (38) may be simplified to the approximate, constant, and periodic Knudsen relation for mixing,

$$\langle M \rangle \approx M_{cp} = s_{\text{in}} s_{\text{out}} Q_r. \tag{39}$$

The latter is the mixing relation which has been derived by MacCready et al. (2018) by assuming periodicity of (33) and approximating the representative inflowing and outflowing salinity variances per unit volume as

$$\begin{aligned} (s'^2)_{\text{in}} &= (s^2)_{\text{in}} - 2s_{\text{in}}\bar{s} + \bar{s}^2 \\ &\approx (s_{\text{in}})^2 - 2s_{\text{in}}\bar{s} + \bar{s}^2, \\ (s'^2)_{\text{out}} &= (s^2)_{\text{out}} - 2s_{\text{out}}\bar{s} + \bar{s}^2 \\ &\approx (s_{\text{out}})^2 - 2s_{\text{out}}\bar{s} + \bar{s}^2, \end{aligned} \tag{40}$$

which is equivalent to $(s^2)_{\text{in}} \approx (s_{\text{in}})^2$ and $(s^2)_{\text{out}} \approx (s_{\text{out}})^2$. The accuracy of the mixing estimates in (37)–(39) is investigated in the following sections.

Mixing relations could also be derived from the salinity variance equation in (33), but they would be more difficult to apply to observations. Even for periodic conditions or long averaging periods, detailed time-dependent information about the internal salinity field would be needed to calculate the variance flux into the domain. Furthermore, the time dependence of the freshwater inflow is included, as indicated by the third term on the right-hand side of (33), which contains the temporal covariance between the freshwater runoff and the squared mean salinity. Only for constant freshwater runoff this term would simplify to $\langle \bar{s}^2 \rangle Q_r$.

4. Idealized example calculations

Four idealized test cases, two analytical and two numerical, are used here to analyze the performance of the TEF-based Knudsen mixing analysis.

a. *Analytical test cases*

For the two analytical test cases presented here, we prescribe conditions for u and s at the estuarine transect under consideration, in such a way that a specified runoff Q_r is obtained and that the salt budget is closed. The classical estuarine solution by Hansen and Rattray (1965) is not suitable, since its advective salt budget is not closed (e.g., MacCready and Geyer 2010). In these two analytical cases, the estuary itself exists only virtually, without being explicitly considered or calculated. The first analytical test case uses linear and stationary profiles of velocity and salinity to demonstrate that, even under such simple conditions, the consideration of nonconstancy in inflow salinity [$(s_{\text{in}})^2 \neq (s^2)_{\text{in}}$] and outflow salinity [$(s_{\text{out}})^2 \neq (s^2)_{\text{out}}$] is essential. In the second analytical test case, a tidal flow with spatial homogeneity across the investigated

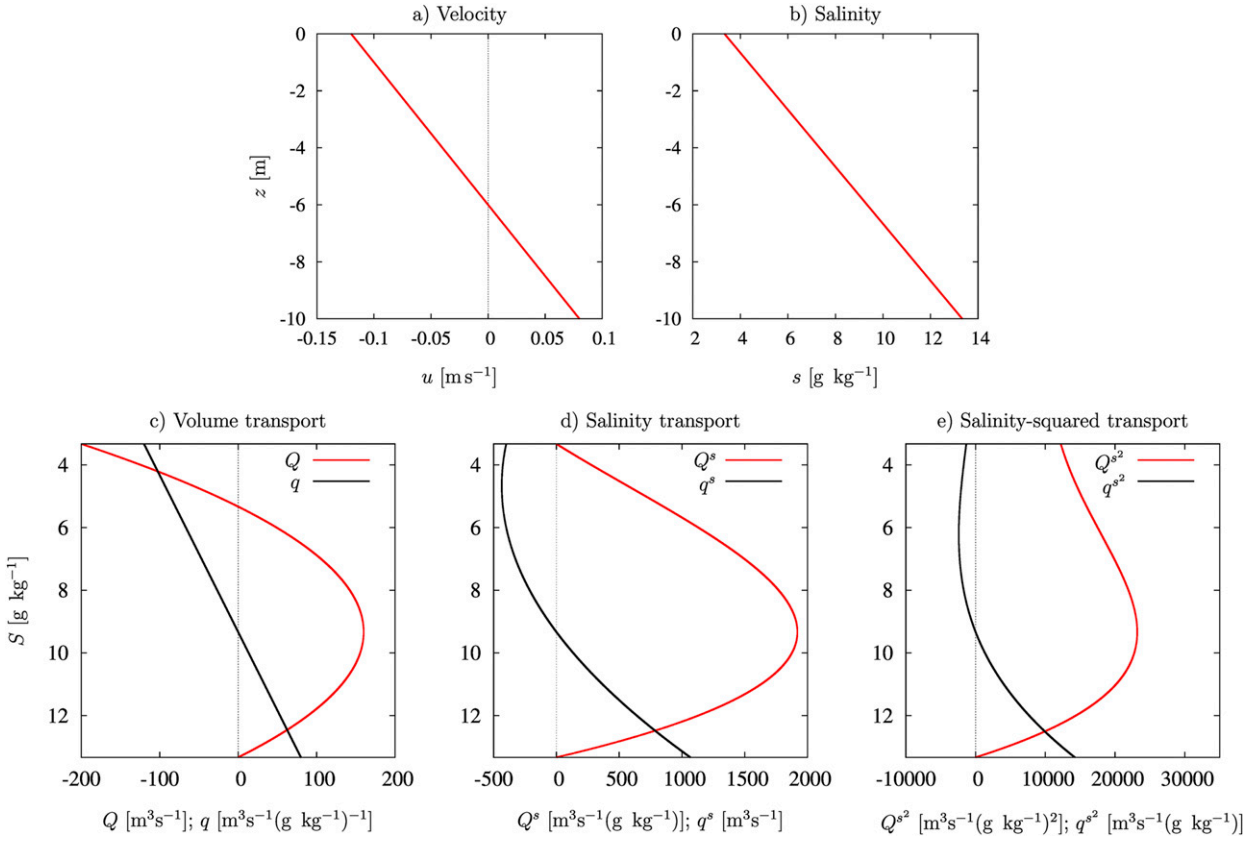

FIG. 2. Linear exchange flow. Profiles of (a) velocity and (b) salinity. (c) Red is volume transport above a certain value of S, $Q(S)$, and black is volume transport per salinity class, $q(S) = -\partial_S Q(S)$. (d) Red is salinity transport above a certain value of S, $Q^s(S)$, and black is salinity transport per salinity class, $q^s(S) = -\partial_S Q^s(S)$. (e) Red is salinity-squared transport above a certain value of S, $Q^{s^2}(S)$, and black is salinity-squared transport per salinity class, $q^{s^2}(S) = -\partial_S Q^{s^2}(S)$.

transect is prescribed, the well-mixed case. This simplest example of a tidally energetic estuary demonstrates that even under these conditions an exchange flow develops, where nonconstancy in inflow and outflow salinities matters.

1) LINEAR EXCHANGE AND SALINITY PROFILE

Assuming a flat-bottom estuarine transect with constant depth H and width W, and a constant net outflow $Q_r = -WHu_r$, the following stationary and laterally homogeneous vertical linear profiles of u and s fulfill volume and salt conservation (see Figs. 2a,b):

$$u(z) = \Delta u\left(-\frac{z}{H} - \frac{1}{2}\right) - u_r;$$
$$s(z) = \Delta s\left(-\frac{z}{H} - \frac{1}{2} + \frac{1}{12}\frac{\Delta u}{u_r}\right), \tag{41}$$

with the bottom to surface velocity and salinity differences Δu and Δs, respectively, where for $\Delta u > 6u_r$ positivity of $s(z)$ is guaranteed. According to (25), we obtain

$$Q(S) = \int_{A(S)} u\, dA = W\int_{z(S_{\max})}^{z(S)} u\, dz, \tag{42}$$

with

$$z(S) = \max\left\{H\left(-\frac{S}{\Delta s} - \frac{1}{2} + \frac{1}{12}\frac{\Delta u}{u_r}\right), 0\right\}, \quad z(S_{\max}) = -H. \tag{43}$$

With this, $q(S)$ results in

$$q(S) = HW\frac{\Delta u}{\Delta s}\left(\frac{S}{\Delta s} - \frac{1}{12}\frac{\Delta u}{u_r} - \frac{u_r}{\Delta u}\right); \tag{44}$$

see Fig. 2c The volume transports result as

$$Q_{\text{in}} = \frac{1}{2}WH\Delta u\left(\frac{u_r}{\Delta u} - \frac{1}{2}\right)^2,$$
$$Q_{\text{out}} = -\frac{1}{2}WH\Delta u\left(\frac{u_r}{\Delta u} + \frac{1}{2}\right)^2, \tag{45}$$

such that volume conservation (1) is fulfilled. Following (25), Q^s, q^s, Q^{s^2}, and q^{s^2} can also be calculated (Figs. 2d,e).

Here, the following parameters have been used: $H = 10\,\mathrm{m}$, $\Delta u = 0.5\,\mathrm{m\,s^{-1}}$, $u_r = 0.02\,\mathrm{m\,s^{-1}}$, $\Delta s = 10\,\mathrm{g\,kg^{-1}}$, $W = 1000\,\mathrm{m}$, and $Q_r = 200\,\mathrm{m^3\,s^{-1}}$.

The resulting Knudsen estimates are summarized here:

$$\begin{aligned} Q_{\mathrm{in}} &= 160\,\mathrm{m^3\,s^{-1}}; & Q_{\mathrm{out}} &= -360\,\mathrm{m^3\,s^{-1}};\\ s_{\mathrm{in}} &= 12.00\,\mathrm{g\,kg^{-1}}; & s_{\mathrm{out}} &= 5.33\,\mathrm{g\,kg^{-1}};\\ (s^2)^{1/2}_{\mathrm{in}} &= 12.04\,\mathrm{g\,kg^{-1}}; & (s^2)^{1/2}_{\mathrm{out}} &= 5.52\,\mathrm{g\,kg^{-1}};\\ M_e &= M_p = 12\,222\,\mathrm{m^3\,s^{-1}\,(g\,kg^{-1})^2};\\ M_{cp} &= M_c = 12\,800\,\mathrm{m^3\,s^{-1}\,(g\,kg^{-1})^2}, \end{aligned}$$

which implies a mixing completeness of Mc = 44.4% and a mixing estimate error of M_{cp} by about 5%.

2) Oscillating and well-mixed tidal flow

We propose here an analytical test scenario for a well-mixed tidal flow with oscillating salinity, given as

$$\begin{aligned} u(t) &= u_r + u_a \cos(\omega t);\\ s(t) &= s_r + s_a \cos(\omega t + \phi), \end{aligned} \tag{46}$$

with the residual velocity $u_r < 0$, the mean salinity s_r, the velocity and salinity amplitudes $u_a > 0$ and $s_a > 0$ with $s_r - s_a \geq 0$, the tidal frequency $\omega = 2\pi/T$ with the tidal period T, and the tidal phase ϕ. It is assumed that the tidal flow passes through a constant cross-sectional area A. Then the cross-sectionally and tidally averaged salt transport is

$$\frac{1}{T}\int_0^T us\,dt = u_r s_r + \frac{u_a s_a}{2}\cos(\phi), \tag{47}$$

such that zero residual salt transport requires

$$\cos(\phi) = -2\frac{u_r s_r}{u_a s_a}, \quad \text{with} \quad u_a s_a \geq 2|u_r| s_r. \tag{48}$$

The inflow and outflow volume fluxes and salinities, Q_{in}, Q_{out}, s_{in}, s_{out}, $(s^2)_{\mathrm{in}}$, and $(s^2)_{\mathrm{out}}$ are calculated by means of (26) and (27) in sufficient accuracy [see MacCready et al. (2018) for the more accurate dividing-salinity approach]. Figure 3 shows an example for $A = 10\,000\,\mathrm{m^2}$, $u_r = -0.1\,\mathrm{m\,s^{-1}}$ [resulting in $Q_r = 1000\,\mathrm{m\,s^{-1}}$, which in this periodic case equals $-Q(0)$], $u_a = 1\,\mathrm{m\,s^{-1}}$, $s_r = 20\,\mathrm{g\,kg^{-1}}$, and $s_a = 10\,\mathrm{g\,kg^{-1}}$, resulting in $\phi = -1.16 = -0.185 \times 2\pi$ [note that (48) also gives a solution with $\phi > 0$, which, however, is not used here since it results in increasing salinity for negative flow velocity, i.e., ebb flow].

The resulting Knudsen estimates are summarized here:

$$\begin{aligned} Q_{\mathrm{in}} &= 813.240\,\mathrm{m^3\,s^{-1}}; & Q_{\mathrm{out}} &= -1813.240\,\mathrm{m^3\,s^{-1}};\\ s_{\mathrm{in}} &= 28.424\,\mathrm{g\,kg^{-1}}; & s_{\mathrm{out}} &= 12.748\,\mathrm{g\,kg^{-1}};\\ (s^2)^{1/2}_{\mathrm{in}} &= 28.471\,\mathrm{g\,kg^{-1}}; & (s^2)^{1/2}_{\mathrm{out}} &= 13.060\,\mathrm{g\,kg^{-1}};\\ M_e &= M_p = 350\,000\,\mathrm{m^3\,s^{-1}\,(g\,kg^{-1})^2};\\ M_{cp} &= M_c = 362\,346\,\mathrm{m^3\,s^{-1}\,(g\,kg^{-1})^2}, \end{aligned}$$

which implies a mixing completeness of Mc = 44.8% and a mixing estimate error of M_{cp} by about 3.5%.

b. Idealized numerical scenarios

The two numerical estuarine examples presented here both explicitly simulate estuarine mixing and show how this is represented by the TEF-based Knudsen mixing analysis. The first is a vertically integrated and one-dimensional test case with and without explicit physical mixing and with strong numerical mixing, due to the diffusive first-order upstream scheme used. It is demonstrated that the numerical mixing directly calculated equals the net inflow of squared salinity in this periodic scenario, if physical mixing is absent. The second, vertically resolved, two-dimensional test case includes physical mixing parameterized by means of a turbulence closure model. It is shown for this tidal flow scenario how small deviations from periodicity significantly influence the accuracy of the mixing estimates.

1) Periodic one-dimensional estuary

Here, we simulate a one-dimensional estuary by means of the following finite-volume momentum equation,

$$\partial_t(uD) = -gD\partial_x\eta - c_D\frac{|u|u}{D}, \tag{49}$$

where the two terms on the right-hand side are the pressure gradient (with gravitational acceleration $g = 9.81\,\mathrm{m\,s^{-2}}$) and the bottom friction (with the drag coefficient $c_D = 2.5 \times 10^{-3}$), the salinity equation,

$$\partial_t(sD) = -\partial_x[D(us - K_h\partial_x s)], \tag{50}$$

where the term on the right-hand side denotes salinity advection and diffusion, and the surface elevation equation,

$$\partial_t\eta = -\partial_x(uD), \tag{51}$$

where $D = H + \eta$ is the total water depth. The estuary is $L = 100\,\mathrm{km}$ long, $W = 1\,\mathrm{km}$ wide, and the depth decreases linearly from 15 m at the mouth to 5 m at the river end, where a freshwater discharge of $Q_r = -Q(0) = 200\,\mathrm{m^3\,s^{-1}}$ is prescribed. Salinity at the

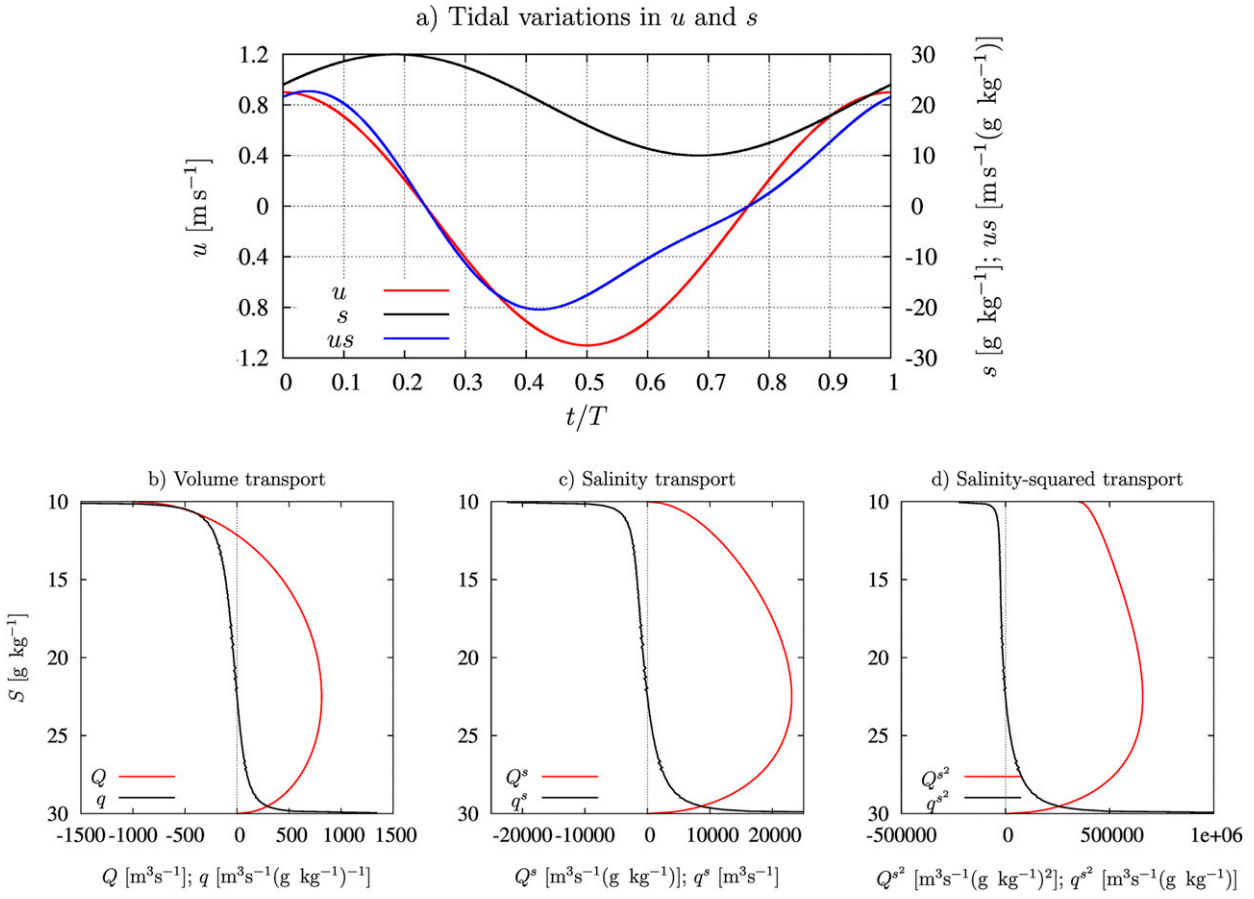

FIG. 3. Oscillating tidal flow. (a) Velocity (red), salinity (black), and salinity flux (blue) time series for the oscillating exchange flow scenario in (46). (b) Red is volume transport above a certain value of S, $Q(S)$, and black is volume transport per salinity class, $q(S) = -\partial_S Q(S)$. (c) Red is salinity transport above a certain value of S, $Q^s(S)$, and black is salinity transport per salinity class, $q^s(S) = -\partial_S Q^s(S)$. (d) Red is salinity-squared transport above a certain value of S, $Q^{s^2}(S)$, and black is salinity-squared transport per salinity class, $q^{s^2}(S) = -\partial_S Q^{s^2}(S)$.

mouth is prescribed as 30 g kg^{-1}, and the tidal elevation amplitude for the harmonic M_2 tide (period $T = 44714$ s) is 2 m. The salinity advection is discretized by means of a first-order upstream scheme, and the salinity diffusion is discretized by central differences:

$$\frac{s_i^{n+1}D_i^{n+1} - s_i^n D_i^n}{\Delta t} = -\frac{D_{i+1/2}^{n+1/2}u_{i+1/2}^{n+1/2}\tilde{s}_{i+1/2}^n - D_{i-1/2}^{n+1/2}u_{i-1/2}^{n+1/2}\tilde{s}_{i-1/2}^n}{\Delta x} + K_h\frac{D_{i+1/2}^{n+1/2}(s_{i+1}^n - s_i^n) - D_{i-1/2}^{n+1/2}(s_i^n - s_{i-1}^n)}{\Delta x^2}, \tag{52}$$

with the interfacial advection salinities

$$\tilde{s}_{i+1/2}^n = \begin{cases} s_i^n & \text{for} \quad u_{i+1/2}^n > 0, \\ s_{i+1}^n & \text{otherwise}, \end{cases} \tag{53}$$

where Δt and Δx denote time step and spatial increment, superscript indices indicate the time step number, and subscript indices indicate the spatial step number. The discrete values for $u_{i+1/2}^{n+1/2}$ are calculated by a straightforward discretization of (49) and the interface depths are defined as $D_{i+1/2}^{n+1/2} = (1/4)(D_i^n + D_{i+1}^n + D_i^{n+1} + D_{i+1}^{n+1})$. The first-order upstream scheme in (53) is known to be highly diffusive and the effective (physical plus numerical) mixing of the advection–diffusion scheme in each grid box at each time step can be calculated numerically exactly according to Klingbeil et al. (2014) as

$$M_i^{n+1/2} = -W\Delta x\left\{\frac{(s_i^{n+1})^2 D_i^{n+1} - (s_i^n)^2 D_i^n}{\Delta t} + \frac{D_{i+1/2}^{n+1/2} u_{i+1/2}^{n+1/2} (\tilde{s}_{i+1/2}^n)^2 - D_{i-1/2}^{n+1/2} u_{i-1/2}^{n+1/2} (\tilde{s}_{i-1/2}^n)^2}{\Delta x}\right.$$
$$\left. - K_h \frac{D_{i+1/2}^{n+1/2}[(s_{i+1}^n)^2 - (s_i^n)^2] - D_{i-1/2}^{n+1/2}[(s_i^n)^2 - (s_{i-1}^n)^2]}{\Delta x^2}\right\} \tag{54}$$

such for tidally periodic conditions the tidally averaged sum of the effective mixing can be quantified as

$$\langle M_{\text{num}}\rangle + \langle M_{\text{phy}}\rangle = \frac{1}{n_{\max}} \sum_{n=1}^{n_{\max}} \sum_{i=1}^{i_{\max}} M_i^{n+1/2}$$
$$= \frac{W}{n_{\max}} \sum_{n=1}^{n_{\max}} \left[u_{1/2}^{n+1/2} (\tilde{s}_{1/2}^n)^2 - K_h \frac{(s_1^n)^2 - (s_0^n)^2}{\Delta x}\right] D_{1/2}^{n+1/2}, \tag{55}$$

assuming that $s_{i_{\max}}^n = \tilde{s}_{i_{\max}+1/2}^n = s_{i_{\max}+1}^n = 0$, since they are located in the freshwater range. In (55) the first term is the numerical mixing $\langle M_{\text{num}}\rangle$ and the second term is the physical mixing $\langle M_{\text{phy}}\rangle$.

For no explicit longitudinal diffusion ($K_h = 0$), the resulting dynamics of this simple numerical estuary is shown in Fig. 4 for $\Delta t = T/1000$ and $\Delta x = L/100$. Tidal velocity and salinity are highly variable and lead to a salt intrusion over the first half (50 km) of the estuary (Figs. 4a,b). The exchange flow is analyzed at $x = 5$ km (see Figs. 4c–e). It can be seen that the inflow of volume (and consequently also the inflow of salinity, salinity squared, and salinity variance) occurs at a narrow salinity range with $S > 28\,\text{g kg}^{-1}$ ($s_{\text{in}} = 28.5517\,\text{g kg}^{-1}$, $(s^2)_{\text{in}}^{1/2} = 28.5537\,\text{g kg}^{-1}$). In contrast, outflows occur at the broad salinity range between 16 and $28\,\text{g kg}^{-1}$, with a peak at low salinities of around $17\,\text{g kg}^{-1}$ ($s_{\text{out}} = 19.9178\,\text{g kg}^{-1}$, $(s^2)_{\text{out}}^{1/2} = 20.1780\,\text{g kg}^{-1}$). This outflow peak at low salinities can be explained by the relatively low friction which allows the tidal wave to be reflected back from the end of the estuary, such that at late ebb increased outflow occurs. Since $(s_{\text{in}})^2 \approx (s^2)_{\text{in}}$ and $(s_{\text{out}})^2 \approx (s^2)_{\text{out}}$, the two mixing estimates from (38), M_p, and (39), M_{cp}, differ by only 6% (see Table 1). Note that for this periodic scenario $M_e = M_p$ and $M_c = M_{cp}$ hold. The mixing completeness results in Mc = 70%. Figure 4e shows the exchange flow profiles for the square of salinity and the variance per unit volume of salinity in comparison. The variance profiles show a slightly smaller amplitude, since the difference to mean salinity $\bar{s}$ instead of the difference to zero is transported. For both profiles, the values for $S = 0$ are similar, with $Q^{s^2}(0) = \langle M\rangle$ and $Q^{s'^2}(0) = \langle M\rangle - \langle \bar{s}^2\rangle Q_r$ for this simple scenario with constant river runoff [see (33)]. Here, the following mixing relations hold: $\langle M\rangle = \langle M_{\text{num}}\rangle = Q^{s^2}(0) = Q^{s'^2}(0) + \langle \bar{s}^2\rangle Q_r = M_e = M_p$. Table 1 gives an overview of the mixing relations.

When applying a longitudinal diffusivity of $K_h = 100\,\text{m}^2\,\text{s}^{-1}$, the salt wedge extends about 10 km farther into the estuary and salinities at the mouth are closer to the open boundary salinity (not shown). Using the effective flux for salinity and its square according to (17), $F^s = us - K_h \partial_x s$ and $F^{s^2} = us^2 - K_h \partial_x s^2$, exchange profiles including the contribution from the diffusive flux can be computed (see Fig. 5). Compared to the simulation without explicit diffusivity, these profiles are (i) shifted to higher salinities and cover a smaller range (due to the increased salinities at the analyzed location) and (ii) have larger amplitudes (due to the increased fluxes and due to the fact that a smaller salinity range is given). The mixing completeness has increased to 73%. Table 1 shows that total mixing is increased by about 20% in comparison to the scenario with $K_h = 0$. Numerical mixing is strongly reduced, since salinity gradients are smoothed by physical mixing which dominates over numerical mixing now. Also here, the following mixing relations hold: $\langle M\rangle = \langle M_{\text{phy}}\rangle + \langle M_{\text{num}}\rangle = Q^{s^2}(0) = Q^{s'^2}(0) + \langle \bar{s}^2\rangle Q_r = M_e = M_p$ and the constant Knudsen mixing relation derived by MacCready et al. (2018), M_{cp}, approximates that values quite closely.

2) Periodic two-dimensional estuary

Finally, we simulate a periodic two-dimensional width-averaged tidal estuary to compare the estuarine mixing estimates in (36)–(39) with the effective (physical

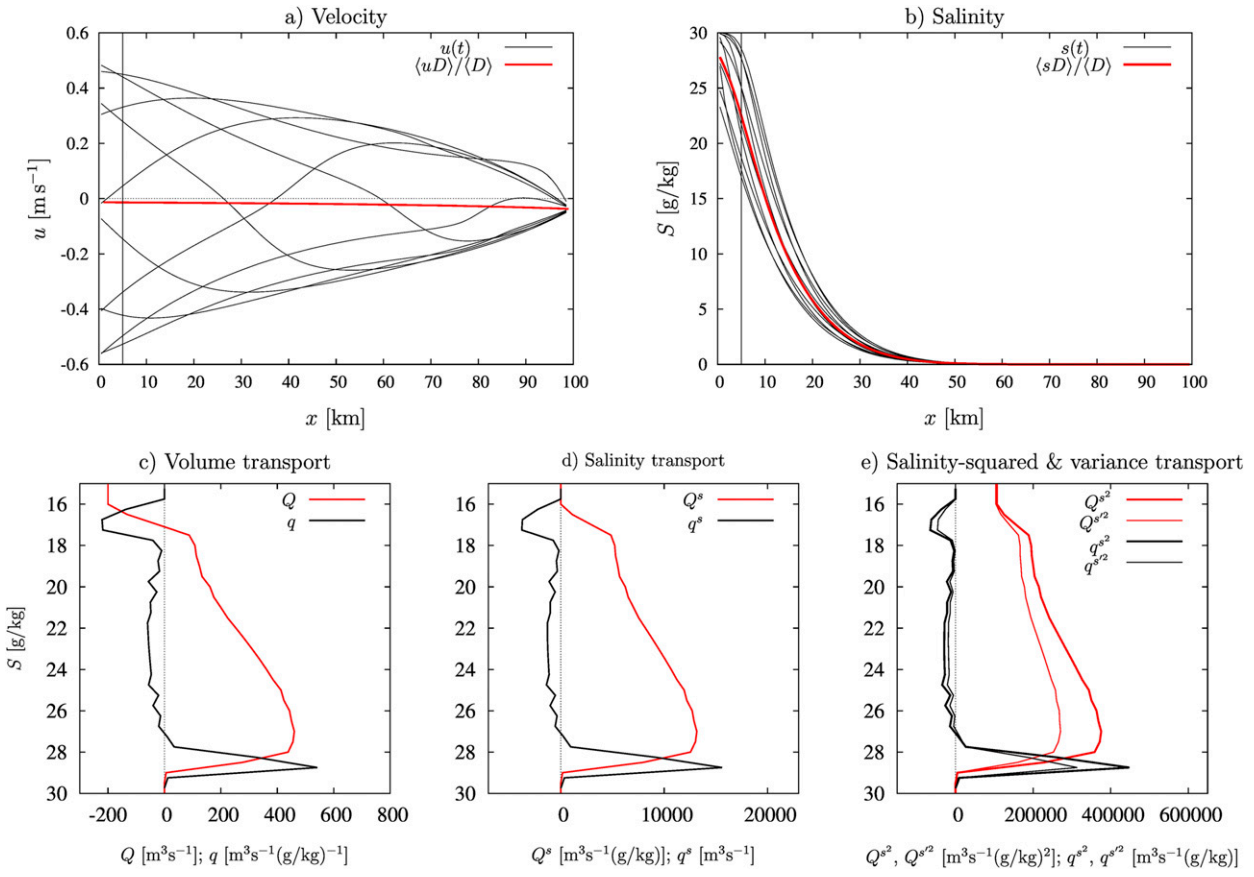

FIG. 4. One-dimensional estuary without explicit longitudinal diffusion. (a) Tidal mean velocity $\langle uD\rangle/\langle D\rangle$ (red) and instantaneous velocity $u(x,t)$ for 10 different tidal phases (black). (b) Tidal mean salinity $\langle sD\rangle/\langle D\rangle$ (red) and instantaneous salinity $s(x,t)$ for 10 different tidal phases (black). Exchange flow profiles at $x = 5$ km [see vertical line in (a) and (b)] with (c) red showing volume transport above a certain value of S, $Q(S)$, and black showing volume transport per salinity class, $q(S) = -\partial_S Q(S)$; (d) red showing salinity transport above a certain value of S, $Q^s(S)$, and black showing salinity transport per salinity class, $q^s(S) = -\partial_S Q^s(S)$; and (e) red showing salinity-squared and variance transport above a certain value of S, $Q^{s^2}(S)$ and $Q^{s'^2}(S)$, and black showing salinity-squared and variance transport per salinity class, $q^{s^2}(S) = -\partial_S Q^{s^2}(S)$ and $q^{s'^2}(S) = -\partial_S Q^{s'^2}(S)$.

plus numerical) tidally averaged mixing integrated over the entire estuary. The setup is similar to the one used by Warner et al. (2005) for evaluating various turbulence closure schemes and by Burchard and Hofmeister (2008) for computing terms in the potential energy anomaly budget.

The idealized estuary is 100 km long and 500 m wide and the depth varies linearly between 15 m at the ocean

TABLE 1. One-dimensional estuary without and with explicit longitudinal diffusion: compilation of the mixing estimates, averaged over one tidal period, and rounded to integer values. For this periodic test case with constant river runoff, the following exact relations hold: $\langle M\rangle = \langle M_{\mathrm{phy}}\rangle + \langle M_{\mathrm{num}}\rangle = Q^{s^2}(0) = Q^{s'^2}(0) + \langle\overline{s}^2\rangle Q_r = M_e$.

Mixing estimate	Variable	Value, $A_h = 0$ [$\mathrm{m^3\,s^{-1}\,(g\,kg^{-1})^2}$]	Value, $A_h = 100\,\mathrm{m^2\,s^{-2}}$ [$\mathrm{m^3\,s^{-1}\,(g\,kg^{-1})^2}$]
Exact mixing	$\langle M\rangle$	106 888	125 963
Physical mixing	$\langle M_{\mathrm{phy}}\rangle$	0	70 646
Numerical mixing	$\langle M_{\mathrm{num}}\rangle$	106 888	55 317
Boundary flux of s^2	$Q^{s^2}(0)$	106 888	125 963
Boundary flux of s'^2, $s > 0$	$Q^{s'^2}(0)$	104 146	119 087
Boundary flux of s'^2, $s = 0$	$\langle\overline{s}^2\rangle Q_r$	2742	6875
Exact Knudsen relation	$M_e = M_p$	106 888	125 963
Constant and periodic relation	$M_c = M_{cp}$	111 737	127 338

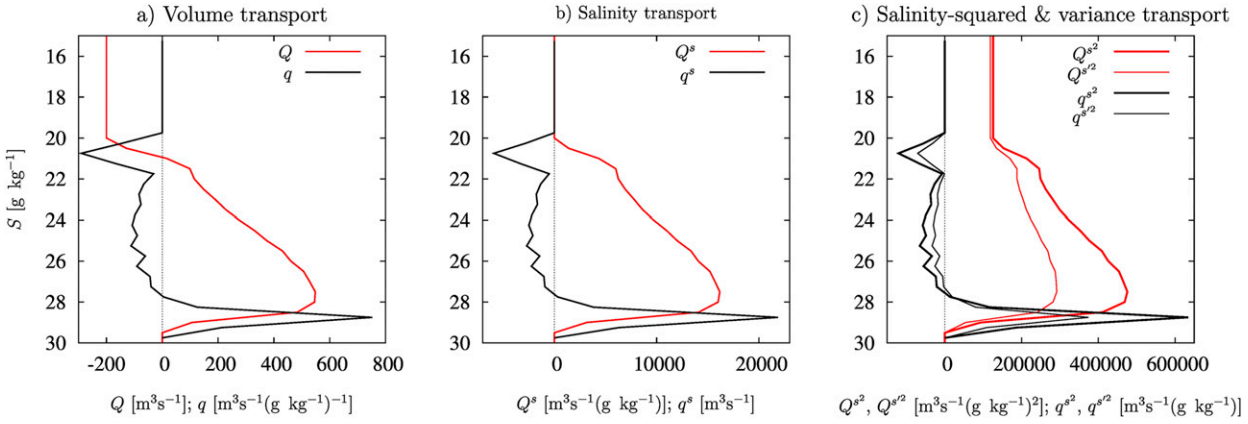

FIG. 5. One-dimensional estuary with explicit longitudinal diffusion $K_h = 100\,\mathrm{m^2\,s^{-1}}$: exchange flow profiles at $x = 5$ km [see vertical line in (a) and (b) of Fig. 4] with (a) red showing volume transport above a certain value of S, $Q(S)$, and black showing volume transport per salinity class, $q(S) = -\partial_S Q(S)$; (b) red showing salinity transport above a certain value of S, $Q^s(S)$, and black showing salinity transport per salinity class, $q^s(S) = -\partial_S Q^s(S)$; and (c) red showing salinity-squared and variance transport above a certain value of S, $Q^{s^2}(S)$ and $Q^{s'^2}(S)$, and black showing salinity-squared and variance transport per salinity class, $q^{s^2}(S) = -\partial_S Q^{s^2}(S)$ and $q^{s'^2}(S) = -\partial_S Q^{s'^2}(S)$.

side (where a constant salinity of $30\,\mathrm{g\,kg^{-1}}$ and a harmonic semidiurnal M_2 tide with an elevation amplitude of 0.6 m are prescribed) and 5 m at the river end (where a constant freshwater runoff of $Q_r = 50\,\mathrm{m^3\,s^{-1}}$ is prescribed). Eddy viscosity and eddy diffusivity are calculated by means of a k–ε two-equation turbulence closure model (Umlauf and Burchard 2005), and explicit longitudinal mixing is neglected. As a numerical model, the General Estuarine Transport Model (GETM; Burchard and Bolding (2002); www.getm.eu) is applied. The simulation uses a temporal discretization with 500 baroclinic and 5000 barotropic time steps for one tidal period, 40 equidistant σ layers in the vertical, and 200 equidistant spatial steps along the estuary. As advection scheme for momentum and salinity, the Superbee scheme is used, implemented by means of a directional-split method (Pietrzak 1998), which is known for its antidiffusive properties (Klingbeil et al. 2014). The simulation is first run for 100 tidal periods which results in an almost periodic state. A perfect periodic state is, however, not approximated, due to the occurrence of internal waves with a frequency different from the tidal frequency. Initialized with this almost periodic solution, the time-averaged mixing during 10 tidal periods is finally evaluated. For this, the cross section at $x = 22.5$ km is evaluated, since it is neither directly influenced by the open boundary conditions (maximum salinity in that cross section does not reach the boundary value) nor situated in the freshwater range at any time. Estuary-integrated parameters are then calculated for $22.5 \le x \le 100$ km.

Figure 6 shows snapshots of salinity and current velocity at full flood and full ebb as well as physical and numerical mixing at full ebb (where the physical mixing has its maximum in this simple tidal estuary without lateral variation). These 10 tidal periods under investigation are time dependent in the sense that the volume, salt, and salt-squared storage terms amount to $V_{\mathrm{stor}} = 0.0219\,\mathrm{m^3\,s^{-1}}$, $S_{\mathrm{stor}} = -8.26\,\mathrm{m^3\,s^{-1}\,g\,kg^{-1}}$, and $(S^2)_{\mathrm{stor}} = -137\,\mathrm{m^3\,s^{-1}\,(g\,kg^{-1})^2}$.

Exchange flow profiles at $x = 22.5$ km are shown in Fig. 7. The profiles of q, q^s, q^{s^2} and $q^{s'^2}$ show significant oscillations in the range of medium salinities between 12 and $18\,\mathrm{g\,kg^{-1}}$, which can be explained by the internal waves moving at the salinity interface. As already in Fig. 4e, also here the amplitude of the salinity variance transport is smaller than for the salinity square (see Fig. 7c). The volume transport integrated over all salinity classes results in $Q(0) = -Q_r + V_{\mathrm{stor}} = -49.9781\,\mathrm{m^3\,s^{-1}}$, the integrated salinity transport is $Q^s(0) = S_{\mathrm{stor}} = -8.26\,\mathrm{m^3\,s^{-1}\,g\,kg^{-1}}$, and the salinity square transport is $Q^{s^2}(0) = \langle M\rangle + (S^2)_{\mathrm{stor}} = 12\,873\,\mathrm{m^3\,s^{-1}(g\,kg^{-1})^2}$. The salinity variance transport is $Q^{s'^2}(0) = \langle M\rangle - \langle\overline{s^2}\rangle Q_r + (S'^2)_{\mathrm{stor}} = 12\,438\,\mathrm{m^3\,s^{-1}(g\,kg^{-1})^2}$ $\mathrm{m^3\,s^{-1}\,(g\,kg^{-1})^2}$ (see Table 2).

The resulting values for the inflow and outflow salinities are $s_{\mathrm{in}} = 20.48\,\mathrm{g\,kg^{-1}}$, $s_{\mathrm{out}} = 14.04\,\mathrm{g\,kg^{-1}}$, $(s^2)^{1/2}_{\mathrm{in}} = 20.51\,\mathrm{g\,kg^{-1}}$, and $(s^2)^{1/2}_{\mathrm{out}} = 14.34\,\mathrm{g\,kg^{-1}}$, such that the mixing completeness amounts to Mc = 69%.

Using the numerical analysis methods by Klingbeil et al. (2014), tidally averaged physical and numerical mixing is estimated as $\langle M_{\mathrm{phy}}\rangle = 13\,458\,\mathrm{m^3\,s^{-1}(g\,kg^{-1})^2}$ and $\langle M_{\mathrm{num}}\rangle = -448\,\mathrm{m^3\,s^{-1}(g\,kg^{-1})^2}$, where the negative numerical mixing appears due to the antidiffusive properties of the Superbee advection scheme. With this, the effective total mixing is $\langle M\rangle = 13\,009\,\mathrm{m^3\,s^{-1}(g\,kg^{-1})^2}$, which is identical to the value resulting from the tidally averaged and vertically integrated advective fluxes

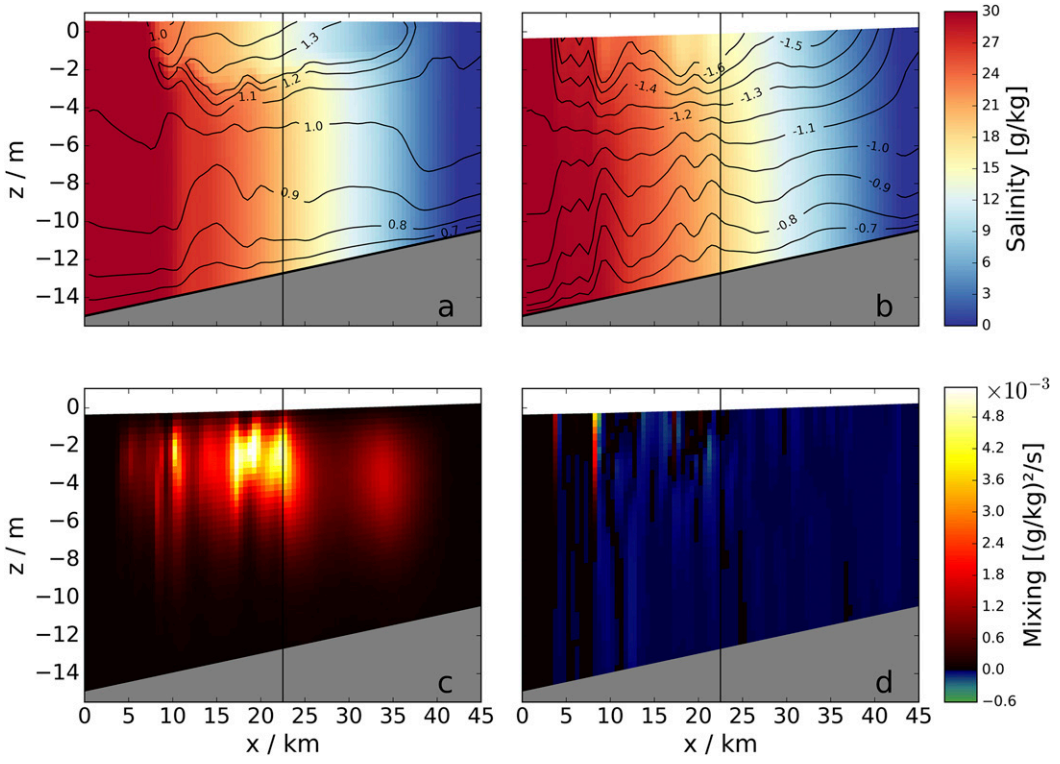

FIG. 6. Periodic two-dimensional estuary, brackish region: (a) salinity (color shading) and current velocity (contour lines) at full flood, (b) salinity and current velocity at full ebb, (c) physical mixing per unit volume at full ebb, and (d) numerical mixing per unit volume at full ebb. The vertical black line at $x = 22.5$ km indicates the location for the TEF analysis.

of S^2 through the open boundary, corrected by the storage of $(S^2)_{\text{stor}}$. The estimate from the nonconstant and nonperiodic Knudsen relation for mixing, M_e from (36), is identical to this value as well, whereas the constant and nonperiodic estimate, M_c from (37) based on $(s^2)_{\text{in}} \approx (s_{\text{in}})^2$ and $(s^2)_{\text{out}} \approx (s_{\text{out}})^2$, amounts to $M_c = 14\,221\,\text{m}^3\,\text{s}^{-1}\,(\text{g}\,\text{kg}^{-1})^2$, which is an overestimation by 9.3%. For the estimates ignoring time dependence [assuming $V_{\text{stor}} = S_{\text{stor}} = (S^2)_{\text{stor}} = 0$], the nonconstant relation from (38) gives $M_p = 13\,154\,\text{m}^3\,\text{s}^{-1}\,(\text{g}\,\text{kg}^{-1})^2$ [i.e., an overestimation by 1% due to the dominance of the negative second term in (36) over the positive third term] and the constant and periodic relation from (39) gives $M_{cp} = 14\,376\,\text{m}^3\,\text{s}^{-1}\,(\text{g}\,\text{kg}^{-1})^2$ (i.e., an overestimation by 10.5%). As an overview, all mixing estimates for averaging over 10 tidal periods are compiled in Table 2.

Realistic applications are generally far away from stationary or periodic conditions, due to the relevance of more than one tidal constituent or dominating effects of fluctuations in wind or river runoff. Therefore, the dependence of the four TEF-based Knudsen mixing estimates on the averaging period is shown in Fig. 8. For averaging over full tidal cycles, all estimates are within about 15%, and none of the approximate relations M_c, M_p, and M_{cp} is generally closer to the exact value $M_e = \langle M \rangle$ than the others. However, when averaging over fractional tidal periods, the approximate relations show strong fluctuations. For short averaging periods, M_c and M_p even give negative values at times. These two estimates do also show a strong dependence on the exact averaging period when it is close to full tidal cycles. In a real situation with various tidal frequencies, this could lead to strong inaccuracies of these relations. By definition, only the exact relation M_e and the constant and periodic relation M_{cp} are constrained to give nonnegative values. This underlines the usefulness and robustness of the simple relation $M_{cp} = s_{\text{in}} s_{\text{out}} Q_r$ derived by MacCready et al. (2018).

5. Discussion

The theory developed here provides a generalization of the total exchange flow (TEF) analysis framework first developed by MacCready (2011) and later extended by MacCready et al. (2018) to estimate mixing. This generalization includes several aspects.

First of all, TEF profiles are defined in (25) for an arbitrary tracer c, as already proposed by Walin (1977).

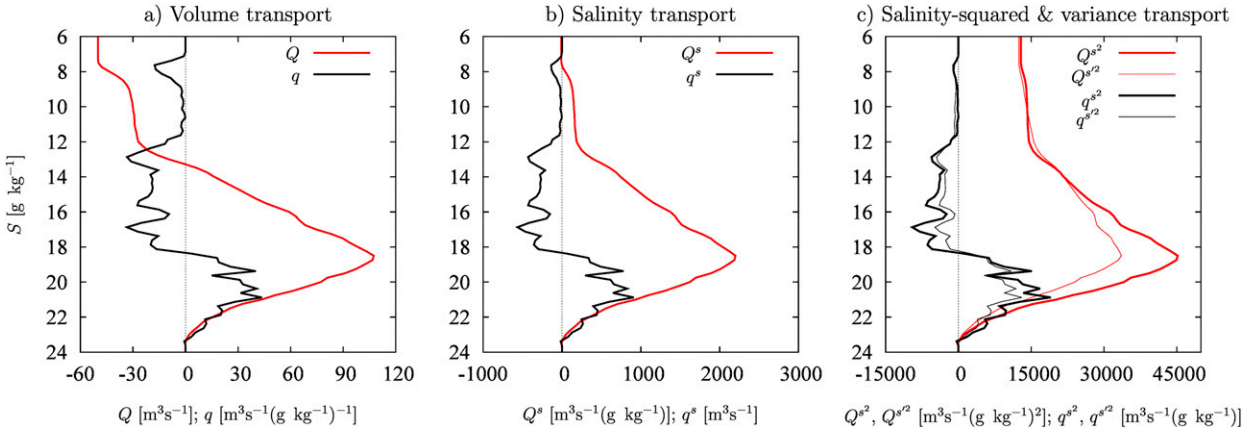

FIG. 7. Periodic two-dimensional estuary: Exchange flow profiles averaged over ten tidal periods almost in periodic equilibrium, evaluated at $x = 22.5$ km (see the vertical lines in Fig. 6) with (a) red showing volume transport above a certain value of S, $Q(S)$, and black showing volume transport per salinity class, $q(S) = -\partial_S Q(S)$; (b) red showing salinity transport above a certain value of S, $Q^s(S)$, and black showing salinity transport per salinity class, $q^s(S) = -\partial_S Q^s(S)$; (c) red showing salinity-squared and variance transport above a certain value of S, $Q^{s^2}(S)$ (thick line) and $Q^{s'^2}(S)$ (thin line), and black showing salinity-squared and variance transport per salinity class, $q^{s^2}(S) = -\partial_S Q^{s^2}(S)$ (thick line) and $q^{s'^2}(S) = -\partial_S Q^{s'^2}(S)$ (thin line).

This has been used here to include TEF profiles also for the square and the variance of salinity, but this might also be interesting for budgeting nutrients, heat, or particulate matter in estuaries. These generalized TEF profiles allow for the consistent calculation of inflow and outflow values in terms of the Knudsen relations [see (26) and (27)]. Based on volume-integrated scalar equations, exact Knudsen-type budgets for these scalars can be formulated, including temporal changes (storage), net transports at the freshwater and the marine boundaries, and internal transformations [see (30)–(33)]. These budgets for volume and salt are identical to the Knudsen relations, as already shown by MacCready (2011). The resulting salinity variance budget in (33) is equal to the budget derived by MacCready et al. (2018), apart from the effect of temporal covariance between runoff and mean salinity square. As sink term, the volume-integrated mixing is included in the salinity variance budget. Assuming stationarity or periodicity and further simplifying this equation, MacCready et al. (2018) derived their simple estuarine mixing estimate, that is, that mixing is approximately the product of inflowing and outflowing salinity and river runoff, which is represented by the mixing estimate M_{cp} defined in (39).

Deriving a budget for the salinity square instead of the salinity variance gives a simpler exact relation for the volume-integrated mixing, now without the necessity to consider the mean salinity of the estuary [see (32) and also Burchard and Rennau (2008)]. In combination with the volume and the salt budget, an exact mixing estimate is obtained, only including inflow and outflow values of salinity and its square, the river runoff, and the storage

TABLE 2. Periodic two-dimensional estuary: compilation of the mixing estimates, averaged over 10 tidal periods, and rounded to integer values. The following exact relations hold: $\langle M\rangle = \langle M_{\rm phy}\rangle + \langle M_{\rm num}\rangle = Q^{s^2}(0) - (S^2)_{\rm stor} = Q^{s'^2}(0) + \langle\bar{s}^2\rangle Q_r - (S'^2)_{\rm stor} = M_e$.

Mixing estimate	Variable	Value [$\mathrm{m^3\,s^{-1}\,(g\,kg^{-1})^2}$]
Exact mixing	$\langle M\rangle$	13 009
Physical mixing	$\langle M_{\rm phy}\rangle$	13 458
Numerical mixing	$\langle M_{\rm num}\rangle$	−448
Boundary flux s^2	$Q^{s^2}(0)$	12 873
Storage of s^2	$-(S^2)_{\rm stor}$	137
Boundary flux of s'^2 for $s > 0$	$Q^{s'^2}(0)$	12 438
Boundary flux of s'^2 for $s = 0$	$\langle\bar{s}^2\rangle Q_r$	456
Storage of s'^2	$-(S'^2)_{\rm stor}$	116
Exact Knudsen relation	M_e	13 009
Constant Knudsen relation	M_c	14 221
Stationary Knudsen relation	M_p	13 154
Constant and periodic Knudsen relation	M_{cp}	14 376

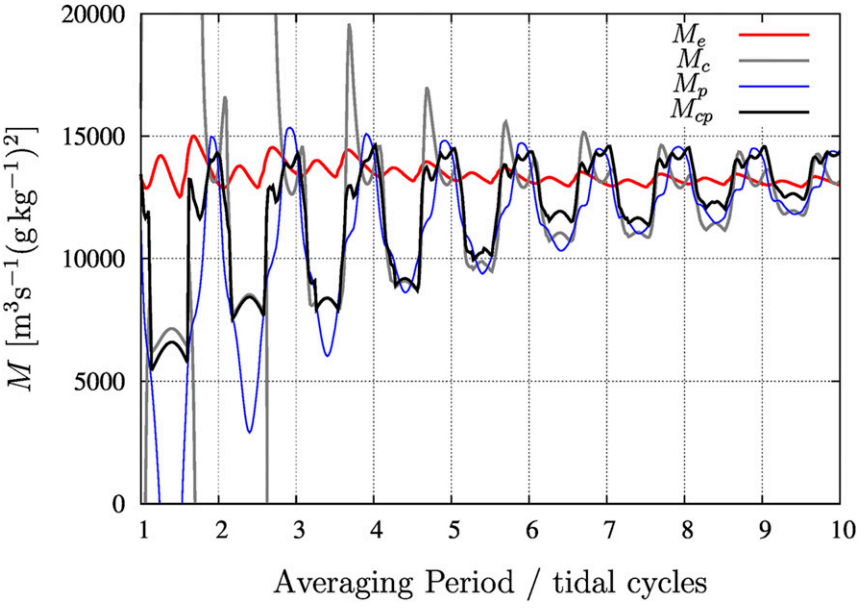

FIG. 8. Periodic two-dimensional estuary, TEF-based Knudsen estimates in (36)–(39) for mixing as a function of the length of the averaging period: exact nonconstant and nonperiodic relation M_e (red); approximate, constant, and nonperiodic relation M_c (gray); approximate, nonconstant, and periodic relation M_p (blue); and approximate, constant, and periodic relation M_{cp} (black).

terms for volume, salt and salt square [see (36)]. Two approximations, 1) periodicity, that is, vanishing storage terms, and 2) constancy of inflow and outflow salinities, that is, $(s^2)_{\text{in}} = (s_{\text{in}})^2$ and $(s^2)_{\text{out}} = (s_{\text{out}})^2$, lead to the simple mixing estimate by MacCready et al. (2018). The exact mixing estimate from (36), relaxed by either approximate 1 or 2, leads to intermediate mixing estimates that may be useful in specific idealized scenarios. While constancy is fulfilled for the simple box estuary scenario discussed in section 2, it is violated in basic analytical cases with stationary and linear profiles of velocity and salinity and periodic and cross-sectionally constant velocity and salinity distributions. In these cases, the assumption of constancy leads to an error in mixing estimates of the order of 5%. A similar error was observed for the one-dimensional numerical estuary, whereas the linearization error was about 10% in the two-dimensional estuary scenario. Whereas the exact mixing estimate in (36) is positive by definition and the simple mixing estimate in (39) is positive by construction, the nonperiodic but constant estimate in (37) and the nonconstant but periodic estimate in (38) may result in negative estimates. This highlights the robustness and usefulness of the simple mixing estimate in (39) proposed by MacCready et al. (2018).

Diffusive fluxes in addition to the advective fluxes across the marine boundary of the estuary are now included in the TEF analysis. Since formally the boundary of the estuary for the TEF analysis can be located anywhere and the boundary area for the TEF analysis might be wide and allowing for horizontal eddy mixing, the inclusion of diffusive fluxes may be essential. Also for idealized models of estuaries, longitudinal diffusivity is often applied to parameterize effects of lateral or vertical shear dispersion (Okubo 1973; Fischer 1976); see also the example of the one-dimensional estuary of the present study.

Since closed budgets of estuarine mixing can only be obtained by means of numerical modeling which inherently includes numerical mixing, the TEF theory has been formulated here such that numerically accurate formulations are applied. Based on the numerical mixing theory developed by Klingbeil et al. (2014), mixing estimates are numerically exact in the sense that they reproduce the effective (physical plus numerical) mixing of the model. This has been demonstrated here for the one-dimensional and two-dimensional test scenarios.

6. Conclusions

The Knudsen-type estuarine mixing estimates derived here could be applied to analyze model simulations using any numerical model. Since most coastal ocean models are based on a finite-volume type of spatial discretization, the exact mixing estimate in (36) could be exactly reproduced numerically as shown in Tables 1

and 2. Such an analysis could be performed not only for one specific transect located somewhere near the mouth of the estuary, but for several transects separating the estuary into finite-volume compartments as demonstrated by Wang et al. (2017). This would help to study the exchange flow and effective (physical plus numerical) mixing characteristics of different regions in the estuary.

Since the robust mixing estimate M_{cp} by MacCready et al. (2018) has generally been proven to show an error of at most 10% from the real mixing, it will for many real estuaries give a first rule-of-thumb estimate of the long-term-averaged basinwide mixing, as the classical case of the Baltic Sea shows (section 2). However, variability in time and space will only be recovered by the more complete mixing estimates considering nonconstancy of inflows and outflows as well as storage terms for volume, salt, and salt squared.

There is a challenge left for the future which has not been tackled here. The exchange of volume across the air–sea interface as given by the net effect of precipitation and evaporation is ignored here. This may be acceptable for classical estuaries in humid regions, but for large estuaries such as the Baltic Sea (Reissmann et al. 2009; Burchard et al. 2018) this may result in large errors in the mixing calculation. Precipitation may actually be included as an additional source of freshwater accounted for by Q_r. However, for inverse estuaries where the river runoff may almost vanish and evaporation dominates substantially over precipitation, such as the Persian Gulf (Kämpf and Sadrinasab 2006) or Shark Bay in Western Australia (Hetzel et al. 2015), the current method will fail; for example, the simple mixing estimate (39) introduced by MacCready et al. (2018) would result in negative mixing (if using negative surface-area-integrated evaporation as river runoff).

Acknowledgments. This paper is a contribution to the Collaborative Research Centre TRR 181 on Energy Transfer in Atmosphere and Ocean (HB and KK) and the Research Training Group Baltic TRANSCOAST GRK 2000 (HB and XL), both funded by the German Research Foundation. PM was supported by Grant OCE-1736242 from the National Science Foundation. The authors are grateful for the constructive comments by Rob Hetland (Texas A&M) and another reviewer.

REFERENCES

Burchard, H., and K. Bolding, 2002: GETM—A general estuarine transport model. Scientific documentation. Tech. Rep. EUR 20253 EN, European Commission, 157 pp.

——, and R. Hofmeister, 2008: A dynamic equation for the potential energy anomaly for analysing mixing and stratification in estuaries and coastal seas. *Estuarine Coastal Shelf Sci.*, **77**, 679–687, https://doi.org/10.1016/j.ecss.2007.10.025.

——, and H. Rennau, 2008: Comparative quantification of physically and numerically induced mixing in ocean models. *Ocean Modell.*, **20**, 293–311, https://doi.org/10.1016/j.ocemod.2007.10.003.

——, F. Janssen, K. Bolding, L. Umlauf, and H. Rennau, 2009: Model simulations of dense bottom currents in the western Baltic Sea. *Cont. Shelf Res.*, **29**, 205–220, https://doi.org/10.1016/j.csr.2007.09.010.

——, and Coauthors, 2018: The Knudsen theorem and the total exchange flow analysis framework applied to the Baltic Sea. *Prog. Oceanogr.*, **165**, 268–286, https://doi.org/10.1016/j.pocean.2018.04.004.

Fischer, H. B., 1976: Mixing and dispersion in estuaries. *Annu. Rev. Fluid Mech.*, **8**, 107–133, https://doi.org/10.1146/annurev.fl.08.010176.000543.

Hansen, D. V., and M. Rattray, 1965: Gravitational circulation in straits and estuaries. *J. Mar. Res.*, **23**, 104–122.

Hetland, R. D., and W. R. Geyer, 2004: An idealized study of the structure of long, partially mixed estuaries. *J. Phys. Oceanogr.*, **34**, 2677–2691, https://doi.org/10.1175/JPO2646.1.

Hetzel, Y., C. Pattiaratchi, R. Lowe, and R. Hofmeister, 2015: Wind and tidal mixing controls on stratification and dense water outflows in a large hypersaline bay. *J. Geophys. Res. Oceans*, **120**, 6034–6056, https://doi.org/10.1002/2015JC010733.

Kämpf, J., and M. Sadrinasab, 2006: The circulation of the Persian Gulf: A numerical study. *Ocean Sci.*, **2**, 27–41, https://doi.org/10.5194/os-2-27-2006.

Klingbeil, K., M. Mohammadi-Aragh, U. Gräwe, and H. Burchard, 2014: Quantification of spurious dissipation and mixing—Discrete variance decay in a finite-volume framework. *Ocean Modell.*, **81**, 49–64, https://doi.org/10.1016/j.ocemod.2014.06.001.

——, F. Lemarié, L. Debreu, and H. Burchard, 2018: The numerics of hydrostatic structured-grid coastal ocean models: State of the art and future perspectives. *Ocean Modell.*, **125**, 80–105, https://doi.org/10.1016/j.ocemod.2018.01.007.

Knudsen, M., 1900: Ein hydrographischer Lehrsatz. *Ann. Hydrogr. Marit. Meteor.*, **28** (7), 316–320.

Lesieur, M., 1997: *Turbulence in Fluids*. 3rd ed. Fluid Mechanics and Its Applications, Vol. 40, Kluwer Academic Publishers, 515 pp.

MacCready, P., 2011: Calculating estuarine exchange flow using isohaline coordinates. *J. Phys. Oceanogr.*, **41**, 1116–1124, https://doi.org/10.1175/2011JPO4517.1.

——, and W. R. Geyer, 2010: Advances in estuarine physics. *Annu. Rev. Mar. Sci.*, **2**, 35–58, https://doi.org/10.1146/annurev-marine-120308-081015.

——, ——, and H. Burchard, 2018: Estuarine exchange flow is related to mixing through the salinity variance budget. *J. Phys. Oceanogr.*, **48**, 1375–1384, https://doi.org/10.1175/JPO-D-17-0266.1.

Matthäus, W., and H. Schinke, 1999: The influence of river runoff on deep water conditions of the Baltic Sea. *Hydrobiologia*, **393**, 1–10, https://doi.org/10.1023/A:1003573328473.

Okubo, A., 1973: Effect of shoreline irregularities on streamwise dispersion in estuaries and other embayments. *Neth. J. Sea Res.*, **6**, 213–224, https://doi.org/10.1016/0077-7579(73)90014-8.

Peters, H., and R. Bokhorst, 2000: Microstructure observations of turbulent mixing in a partially mixed estuary. Part I: Dissipation rate. *J. Phys. Oceanogr.*, **30**, 1232–1244, https://doi.org/10.1175/1520-0485(2000)030<1232:MOOTMI>2.0.CO;2.

——, and ——, 2001: Microstructure observations of turbulent mixing in a partially mixed estuary. Part II: Salt flux and stress. *J. Phys. Oceanogr.*, **31**, 1105–1119, https://doi.org/10.1175/1520-0485(2001)031<1105:MOOTMI>2.0.CO;2.

Pietrzak, J., 1998: The use of TVD limiters for forward-in-time upstream-biased advection schemes in ocean modeling. *Mon. Wea. Rev.*, **126**, 812–830, https://doi.org/10.1175/1520-0493(1998)126<0812:TUOTLF>2.0.CO;2.

Ralston, D. K., G. W. Cowles, W. R. Geyer, and R. C. Holleman, 2017: Turbulent and numerical mixing in a salt wedge estuary: Dependence on grid resolution, bottom roughness, and turbulence closure. *J. Geophys. Res. Oceans*, **122**, 692–712, https://doi.org/10.1002/2016JC011738.

Reissmann, J. H., and Coauthors, 2009: Vertical mixing in the Baltic Sea and consequences for eutrophication—A review. *Prog. Oceanogr.*, **82**, 47–80, https://doi.org/10.1016/j.pocean.2007.10.004.

Sun, Q., M. M. Whitney, F. O. Bryan, and Y.-h. Tseng, 2017: A box model for representing estuarine physical processes in Earth system models. *Ocean Modell.*, **112**, 139–153, https://doi.org/10.1016/j.ocemod.2017.03.004.

Umlauf, L., and H. Burchard, 2005: Second-order turbulence models for geophysical boundary layers. A review of recent work. *Cont. Shelf Res.*, **25**, 795–827, https://doi.org/10.1016/j.csr.2004.08.004.

Walin, G., 1977: A theoretical framework for the description of estuaries. *Tellus*, **29**, 128–136, https://doi.org/10.3402/tellusa.v29i2.11337.

——, 1981: On the deep water flow into the Baltic. *Geofysica*, **17**, 75–93.

Wang, T., W. R. Geyer, and P. MacCready, 2017: Total exchange flow, entrainment, and diffusive salt flux in estuaries. *J. Phys. Oceanogr.*, **47**, 1205–1220, https://doi.org/10.1175/JPO-D-16-0258.1.

Warner, J. C., C. R. Sherwood, H. G. Arango, and R. P. Signell, 2005: Performance of four turbulence closure models implemented using a generic length scale method. *Ocean Modell.*, **8**, 81–113, https://doi.org/10.1016/j.ocemod.2003.12.003.